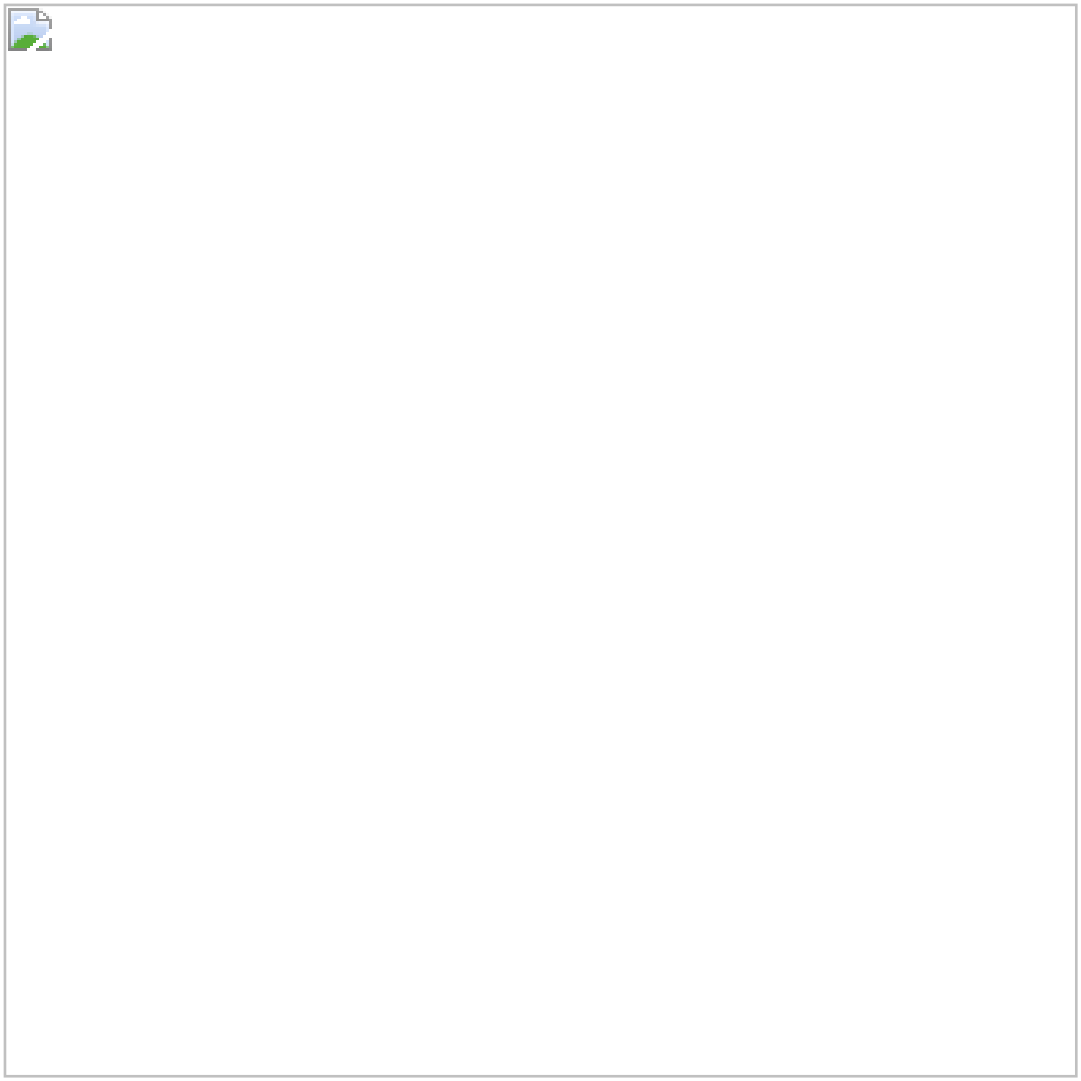

MUDFLOW DISTURBANCE IN LATEST MIOCENE FORESTS IN LEWIS COUNTY, WASHINGTON

Authors: YANCEY, THOMAS E., MUSTOE, GEORGE E., LEOPOLD, ESTELLA B., and HEIZLER, MATT T.

Source: PALAIOS, 28(6) : 343-358

Published By: Society for Sedimentary Geology

URL: https://doi.org/10.2110/palo.2012.p12-063r

PALAIOS
Emphasizing the impact of life on Earth's history

PALAIOS, 2013, v. 28, p. 343–358
Research Article
DOI: 10.2110/palo.2012.p12-063r

1926 SEPM Society for Sedimentary Geology

MUDFLOW DISTURBANCE IN LATEST MIOCENE FORESTS IN LEWIS COUNTY, WASHINGTON

THOMAS E. YANCEY,[1]* GEORGE E. MUSTOE,[2] ESTELLA B. LEOPOLD,[3] and MATT T. HEIZLER[4]

[1]*Geology and Geophysics Department, Texas A&M University, College Station, Texas 77843, USA, tyancey@geos.tamu.edu;* [2]*Geology Department, Western Washington University, Bellingham, Washington 98225, USA, mustoeg@geol.wwu.edu;* [3]*Biology Department, University of Washington, Seattle, Washington 98105, USA, eleopold@u.washington.edu;* [4]*New Mexico Bureau of Geology and Mineral Resources, Socorro, New Mexico 87801, USA, matt@nmt.edu*

ABSTRACT

The lower part of the Wilkes Formation (uppermost Miocene) exposed along lower Salmon Creek in Lewis County, Washington, consists of volcaniclastic-dominated deposits. The section contains a stacked series of volcanic runout mudstone beds overlain by more distal runout mudstone beds, interlayered with carbonaceous mudstone and lignite-woodmat beds that are in turn overlain by poorly sorted volcaniclastic mudstone and sandstone. The section contains a record of forested lowlands inundated by volcanic mudflows, followed sequentially by rising water level associated first with deposition in swamp and lake-margin environments and later by deposition in a lake environment. The lakebed sediments contain common siderite concretions of varied form, including coprolite-shaped concretions that are confined to lakebed deposits. The volcanic mudflow deposits are similar to deposits of mudflows-lahars of modern Cascades stratovolcanoes. Two volcanic ash fall beds contained within lignites in the middle of the section yield $^{40}Ar/^{39}Ar$ radiometric dates. After separation of plagioclase crystals into populations of cloudy appearance (inherited) and clear appearance (newly crystallized), a best age of 6.13 ± 0.08 Ma is determined for the lower ash bed. Sediments contain abundant and well-preserved pollen and spores that document botanical changes progressing from *Nyssa*-dominated to *Taxodium*-dominated to mixed forest assemblages. The existence of *Taxodium* and other warm-climate taxa in the Wilkes Formation indicates the presence of a wet, warm temperate climate in the Puget lowlands during the latest Miocene.

INTRODUCTION

This study examines the depositional and botanical changes in forested lowlands that were inundated by episodic volcanic mudflow (lahar) events at a site in southwest Washington, approximately 50 km northwest of Mount St. Helens (Fig. 1), in the Puget lowlands west of the Cascade Range. These deposits are part of the uppermost Miocene Wilkes Formation, a unit containing a rich and diverse microflora recording the botanical response to mudflow disruption. The stratigraphic section documents changing environmental conditions during a time of rising base level within the depositional basin, culminating in formation of a lake (Roberts, 1958; Mustoe et al., 2009). The processes of sediment deposition are interpreted to be similar to those present in lowlands adjacent to modern stratovolcanoes of the Cascades Range.

The Wilkes Formation has previously received attention from geoscientists because of siderite concretions that have been variously interpreted as vertebrate coprolites (Amstutz, 1958), intestinal casts (Seilacher et al., 2001) or nonbiogenic pseudocoprolites (Spencer, 1993; Mustoe, 2001). Roberts (1958) and Mustoe (2001) reported on locations where *in situ* concretions are abundant. This study provides further documentation of siderite concretions present in the Wilkes Formation and documents features related to their formation and subsequent alteration.

New $^{40}Ar/^{39}Ar$ radiometric dating provides a uppermost Miocene age for the lower part of the Wilkes Formation. This date comes from two volcanic ash fall layers that occur within lignite beds (as tonsteins) in the middle interval of the Lower Horseshoe Bend section and the Red Gate section on Salmon Creek (Figs. 2–3). A preliminary $^{40}Ar/^{39}Ar$ date reported for these ash layers (Yancey and Mustoe, 2007) is replaced with this more accurate analysis. Previous age dating of the Wilkes Formation consists of a late Miocene age determination for the lower part of the formation based on leaf fossils (Roberts, 1958). The new $^{40}Ar/^{39}Ar$ age date is the only reported radiometric age date for the Miocene–Pliocene strata of the southern Puget Lowlands.

STUDY AREA

Wilkes Formation strata studied for this report are exposed in high bluffs along the entrenched lower part of Salmon Creek southeast of the town of Toledo, in southwestern Lewis County, Washington (Fig. 1). The study area is located on the south margin of the Wilkes Hills within Section 34, T.11N, R.1W where strata are well exposed in the Lower Horseshoe Bend section (WWU Site 1571, latitude 46°23.47N, longitude 122°47.73W) and the Red Gate section (WWU Site 2138, latitude 46°23.667N, longitude 122°47.51W), located 0.5 km apart. The Salmon Creek Valley cuts across the Wilkes Hills in this area and Salmon Creek flows within deeply entrenched meanders downcut approximately 10–15 m below the remnants of a former valley bottom, now present as terraces covered with 1–2 m of gravel (Roberts, 1958; Mustoe, 2001; Yancey and Mustoe, 2007). The gravel layer consists of Pleistocene terrace gravel derived from glacial till and outwash of the Pleistocene Logan Hill Formation (Roberts, 1958).

GEOLOGIC SETTING

The Wilkes Formation is a continental sedimentary unit consisting of approximately 230 m of sandstone and mudstone deposited during a time of major structural, volcanic, and depositional change in the Puget lowlands west of the southern Washington Cascades (Roberts, 1958). During the middle Miocene a change occurred, from dominantly basaltic volcanism, probably related to the extrusion of Columbia River Plateau flood basalt, to dominantly andesitic and dacitic volcanism (Roberts, 1958). Coincident with this change in type of volcanism was the formation of a regional northwest–southeast fold system in Washington (Cheney and Hayman, 2007). This was followed by north-south–aligned Cascades uplift that varied from high uplift in the northern Washington Cascades to low uplift in the southern Washington Cascades, and by faulting that is similar in style to Basin and Range deformation (Reiners et al., 2002; Cheney and Hayman, 2007). These volcanic and structural events created a divide between western Washington and central and eastern Washington that shaped the depositional basins of the region. The Wilkes Formation was deposited in response to these major changes and is exposed in the northwest-southeast–trending Napavine syncline (Roberts, 1958).

* Corresponding author.
Published Online: June 2013

 0883-1351/13/0028-0343/$3.00

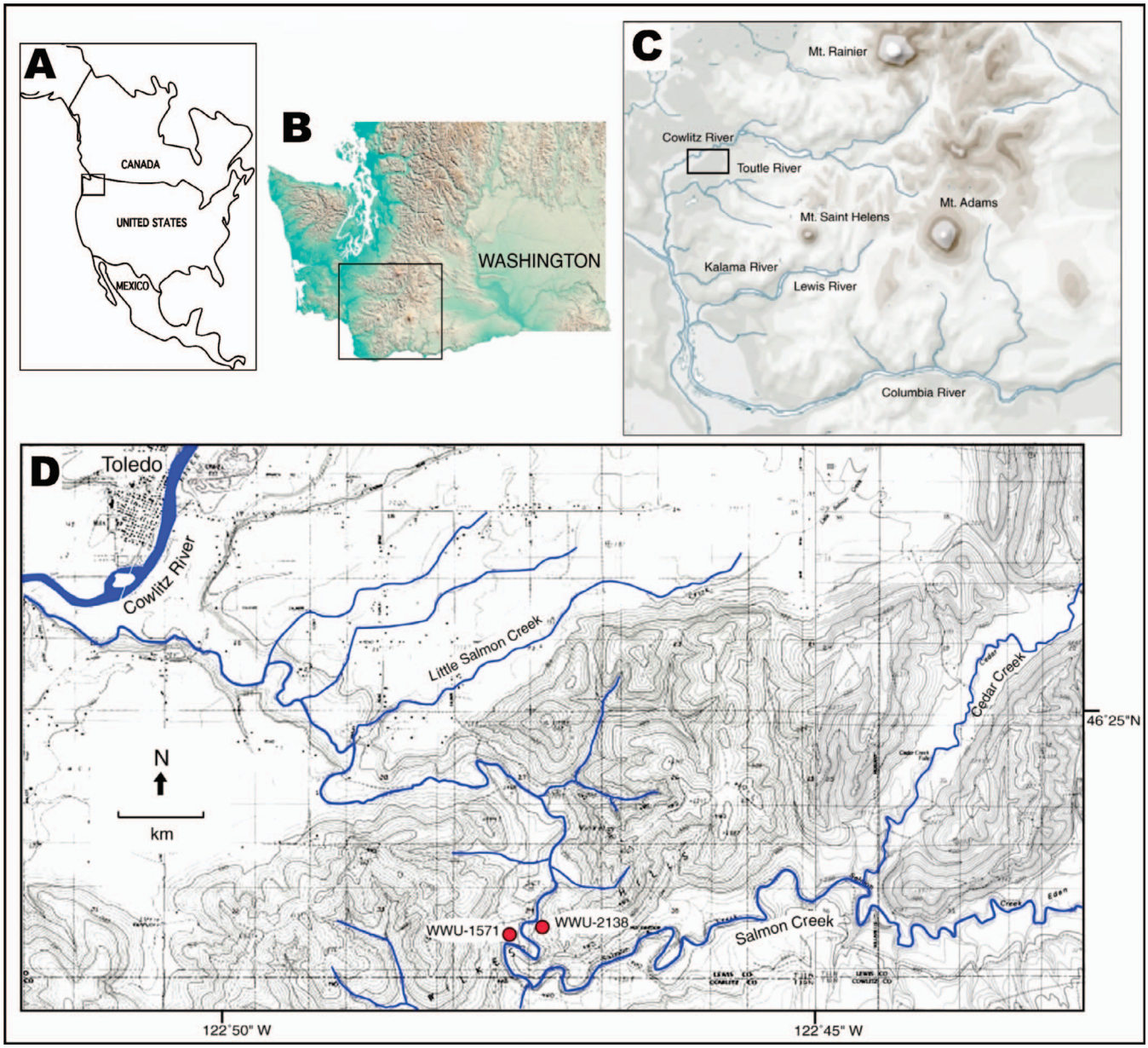

FIGURE 1—Location map of study area. A) North America. B) Washington state in North America. C) Southwestern Washington state. D) Salmon Creek area in Washington state.

The Wilkes Formation thickens northward and is continuous with continental deposits in the adjacent Centralia-Chehalis area (Snavely et al., 1958; Roberts, 1958) and Puyallup River area (Mullineaux et al., 1959). Upper Miocene continental deposits are exposed in the south Puget lowlands along the west margin of the Cascade Range and east of the Willapa Hills part of the Coast Ranges and are coeval with the Montesano Formation of the Grays Harbor area (Snavely et al., 1958). The Puget lowlands area was a structural low in the Middle Miocene, when flood basalt from central Washington flowed west along the Columbia River corridor to the ocean and extended north to the southern Puget lowlands (Tolan et al., 1989; Wells et al., 1989). Deposition of the Wilkes Formation began in the late Miocene when local volcanism in southern Washington shed volcanic sediments to the west and to the east (Roberts, 1958; Mullineaux et al., 1959).

Strata in the lower Wilkes Formation of the Wilkes Hills indicate a low-relief depositional basin, but other parts of the formation contain thick layers of sandstone and thin conglomerate beds (Roberts, 1958) derived from the Cascades to the east and the Green Mountain Range to the south. Deposition of volcanic mudflows probably disrupted drainage patterns and created ponding on lowlands that produced lakes and associated swamps where woody peat accumulated. Continuing uplift of the southern Washington Cascades deformed deposits of the Wilkes Formation (Roberts, 1958) and ended sediment accumulation.

METHODS

Particle size data for the <1 mm fraction of sediment samples in the Salmon Creek stratigraphic section were obtained using a Malvern Mastersizer laser diffraction spectrometer at Western Washington University, supplemented with wet screening of selected samples. Malvern laser diffraction was used for grain size analyses because it produces continuous records of grain size of particles 1 mm and smaller and is best for sediment with high clay-silt content. Sediments that contained visible organic matter were dried at room temperature, then pulverized and heated for several hours at 450 °C to destroy carbonaceous matter. Samples of ~5 g of sediment were suspended

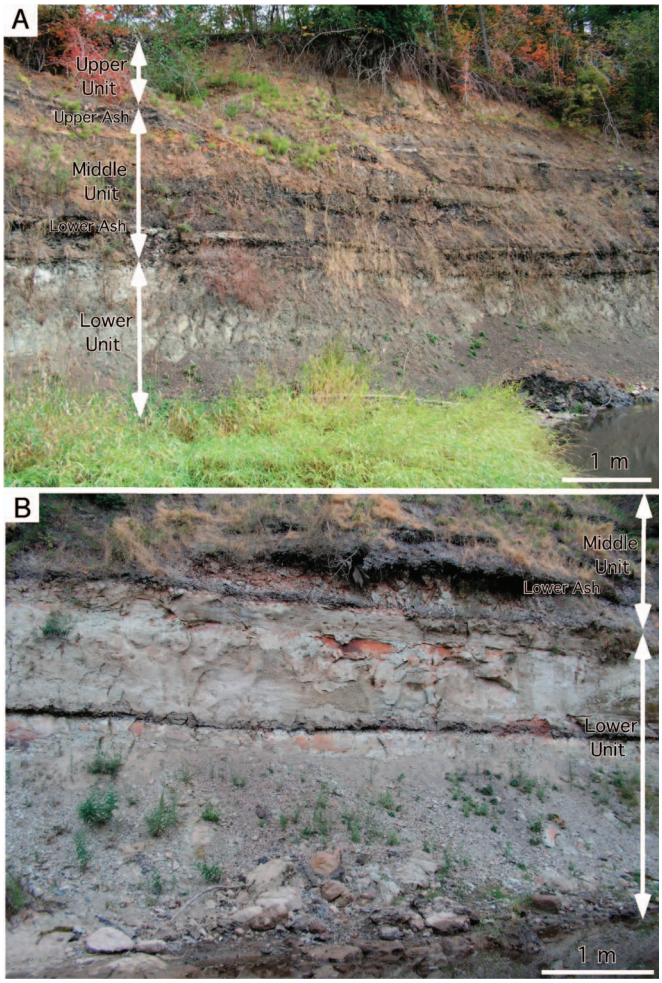

FIGURE 2—Exposures of the lower Wilkes Formation along Salmon Creek, showing three major intervals of deposition. A) The Lower Horseshoe Bend section (WWU site 1571), showing the lower, middle and upper parts of the section and two laterally continuous volcanic ash beds. B) The lower half of the Red Gate section (WWU site 2138) with volcanic mudflows exposed above stream level. Volcanic mudflow unit boundaries in this exposure occur at the conspicuous incised horizons.

using ultrasonification in 20 ml of 0.1% aqueous sodium hexametaphosphate. Grain size data was obtained for the Lower Horseshoe Bend section, but many fine-grained sediments from the Red Gate section did not disaggregate with this procedure.

Grain size distributions made by Malvern laser diffraction and sieving of dispersed mud-rich sediment produced notably different results for mixed grain size sediments, with laser spectrometry (measured as volume percent) consistently recording a finer grain size distribution than sieving (measured as weight percent). Two examples of this difference include measurements of poorly sorted sandy sediment at 12.8 m and 17.2 m in the Lower Horseshoe Bend section. The lower sample has a laser diffraction measure of 17 volume percent sand versus 43.5 weight percent sand measured by sieving, and the upper sample has a laser diffraction measure of 23.5 volume percent sand versus 41.3 weight percent sand. The contrasting results affect determination of processes of sediment deposition under conditions of water transport, but are less important in work with the volcanic mudstone. Visual examination of sand fraction residues was used to identify provenance (volcanic versus reworked sedimentary) of sediment grains and to identify samples unsuitable for Malvern grain size determination because of localized cementation of grains.

Identification of mineral composition of concretions was made by X-ray diffraction on a Rigaku Geigerflex diffractometer using Ni-filtered Cu K-alpha radiation on powdered samples. WDS microprobe analysis was made on a Cameca SX50 microprobe equipped with four wavelength-dispersive spectrometers (WDS) and a Princeton Gamma-Tech energy-dispersive detector system (EDS). Samples studied for this report are kept at Western Washington University (WWU) and Texas A&M University (TAMU).

Most pollen separations were performed at the University of Washington palynology laboratory, except for several pollen samples of the upper part of the upper unit processed in the palynology laboratory at Texas A&M University. Standard palynological procedures for processing fossil pollen were used with the samples. Pollen extraction was done with 2 g of sediment placed in warm 10% HCl for 10 minutes to remove carbonate. The residue was then allowed to react overnight with 30 ml of 48% HF. After washing, the residue was treated for 4 minutes with glacial acetic acid, followed by 10 minute exposure to 1:1 Schultze Solution, followed by 10 minutes in 10% KOH. Samples were screened through 180-mesh Nitex screen and given an optical check. Samples 3, 5, 7, and 9 were treated 10 additional minutes in 10% KOH. Palynomorphs were stained with safranin and permanent slides were prepared using glycerin jelly as a mounting medium, sealing cover slip edges with clear lacquer.

The volcanic ash beds were observed to contain two types of plagioclase feldspar: those with clear appearance and those with cloudy-white appearance. These two types were separated into discrete subsamples for analysis. Due to the young age of the volcanic ash for using the $^{40}Ar/^{39}Ar$ dating method, small crystal size and low K content, it was not possible to date individual crystals. Thus, 10-crystal aliquots of each plagioclase type were carefully handpicked in an effort to obtain age homogeneous crystal groups. Crystal aliquots were degassed in two increments using a CO_2 laser. The first step degassed between ~3% and 32% of the total ^{39}Ar, with the intent of removing the nonradiogenic component from the crystals. The second step fused the grains, and the age results of this B-step are plotted for age analysis (Fig. 4). Hornblende was also separated from the upper ash bed. Two small aliquots (~3 mg) were analyzed. Age spectra for these samples (provided below) give indistinguishable plateau ages.

AGE AND COMPOSITION OF WILKES FORMATION VOLCANIC ASH

The two thin volcanic ash beds were observed to be present in both stratigraphic sections studied, indicating a minimum lateral extent of 0.5 km. The lower volcanic ash has an average thickness of 15 cm whereas the upper volcanic ash has an average thickness of 5 cm. Each ash layer occurs within a lignite bed and was preserved from scour by water currents or erosion, consistent with ash fall deposition from a single volcanic eruption. Major element composition of both ash beds is shown in Table 1. The silica composition lies within the range of dacite magma, but enhanced Al_2O_3 values relative to SiO_2 indicate diagenetic compositional change in the ash (e.g., Clarke, 1924). The abundance of large kaolinite crystals in the ash layers supports this interpretation.

Volcanic ash beds in the Wilkes Formation are crystal rich (Fig. 5F) with abundant phenocrysts of plagioclase (60% anorthite composition) and quartz (commonly occurring as bipyramidal crystals) along with subordinate amounts of green hornblende, minor ilmenite, black mica, and zircon. Glass shards are altered and recrystallized to kaolinite that forms a matrix around the phenocrysts. The lower volcanic ash has a dominant medium sand grain size mode (0.25–0.5 mm) with submodes of 0.040–0.065 mm and 0.5–1 mm; the largest mode includes authigenic vermiform kaolinite crystals. The largest vermiform kaolinite crystals are 1 by 5 mm in size. Scattered large pieces of wood are also present in the ash bed.

Radiometric $^{40}Ar/^{39}Ar$ ages were determined for both ash beds (Fig. 4A) of the Lower Horseshoe Bend section using plagioclase. Although plagioclase-only separations generated a low-resolution age

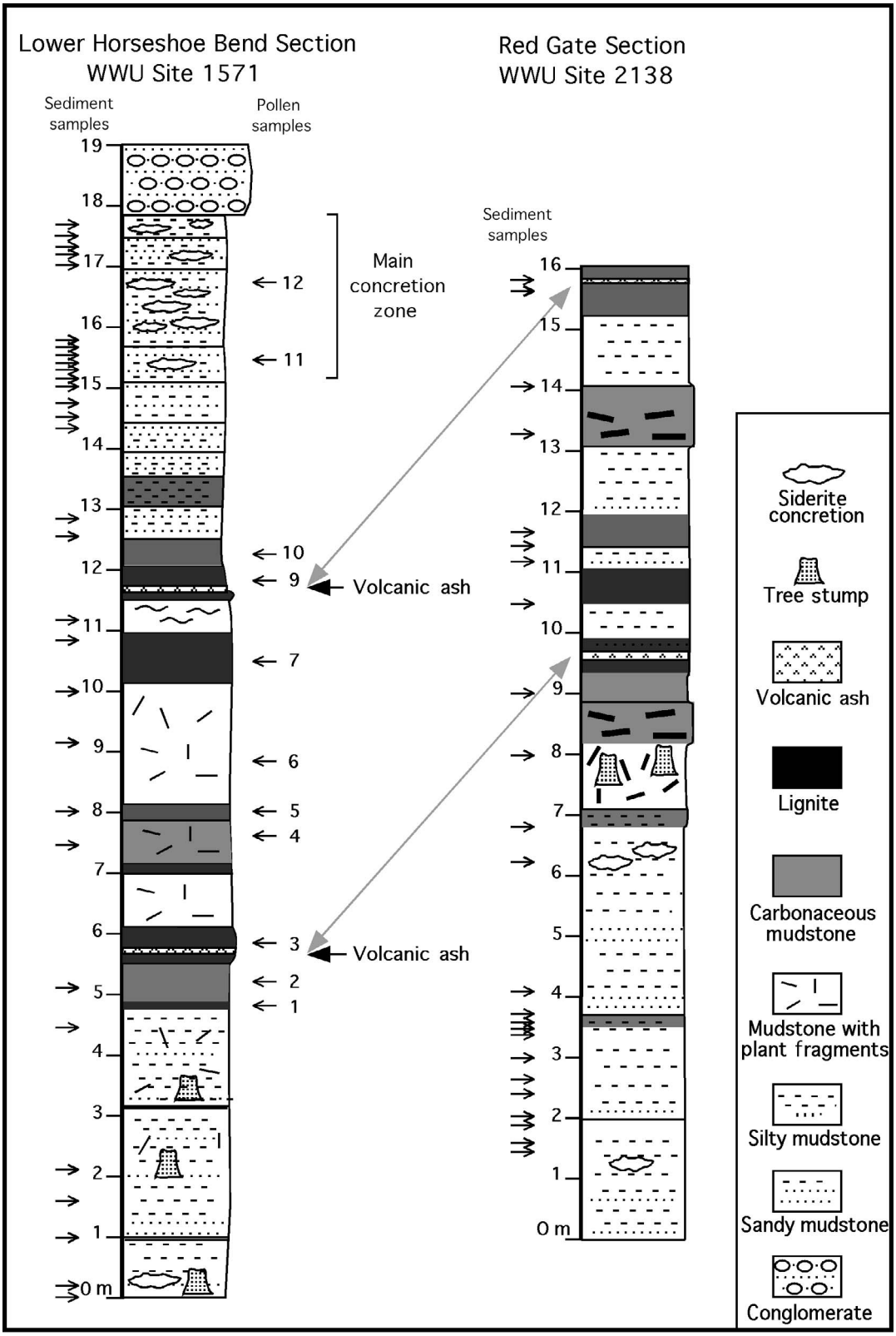

FIGURE 3—Stratigraphic sections of Wilkes Formation in the Lower Horseshoe Bend and Red Gate sections, showing stratigraphic levels of sediment samples and pollen samples and strata with siderite concretions. Correlation between the two sections is fixed by volcanic ash beds and woodmat peat horizons.

determination, high-resolution age determinations were obtained with analysis of separates of clear plagioclase grains. Nineteen separates (16 clear, 3 cloudy) yielded apparent ages between ~6 and 40 Ma, with 11 of the 19 fusions giving a normal distribution of dates at 6.13 ± 0.08 Ma. The three cloudy-white separates are much older at ~15, 26, and 40 Ma. The slight skewing to older ages observed in the latest Miocene cluster is caused by partial contamination of the juvenile feldspar by older crystals. The preferred eruption age of this lower ash is judged to be 6.13 ± 0.08 Ma and is given by the youngest group of the clear grains. Hornblende separated from the upper ash bed also

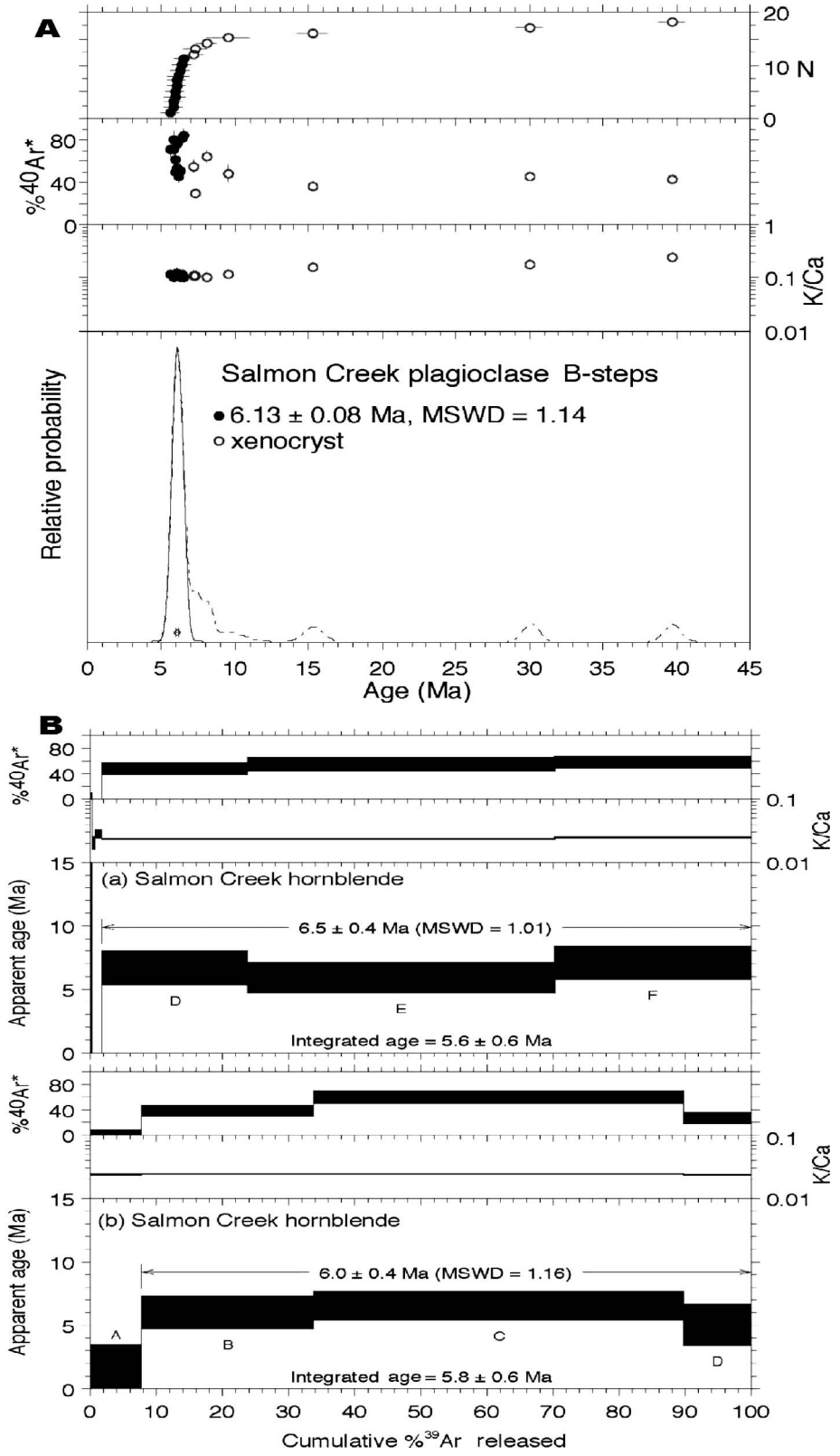

FIGURE 4—A) Relative probability plot for the plagioclase $^{40}Ar/^{39}Ar$ age data from the lower volcanic ash bed. The youngest 11 age results yield a weighted mean eruption age of 6.13 ± 0.08 Ma. Older dates are shown as open symbols and are interpreted to be the result of mixing of inherited older crystals in the phenocryst population. Age data shown are from the second step of the two-step incremental heating procedure and all data are shown with 1 σ error bars. B) Replicate age spectra, K/Ca, and radiogenic $^{40}Ar/^{39}Ar$ yield diagrams for hornblende of the upper volcanic ash bed. Inverse-variance weighted mean combination of replicates 1 and 2, respectively, yield a preferred eruption age of 6.2 ± 0.3 Ma (1 σ).

TABLE 1—Major element composition of Wilkes Formation tephra layers. Determinations by X-ray fluorescence, using Rigaku model 3070 XRF spectrometer, analyzing glass discs prepared by fusing 3.50 g of rock powder with 7.00 g lithium metaborate flux at 1000 °C.

	Lower volcanic ash layer WWU site 1571	Upper volcanic ash layer WWU site 2138
Oxide	Weight %	Weight %
SiO_2	57.22	47.56
Al_2O_3	24.86	36.62
TiO_2	0.93	1.01
Fe_2O_3*	2.61	1.25
MnO_2	0.04	0.00
CaO	5.29	1.18
K_2O	0.05	0.00
P_2O_5	0.00	0.00
MgO	1.02	0.13
Na2O	3.38	0.70
Loss on ignition**	3.82	12.06
Total	99.22	100.53

* Total iron calculated as Fe_2O_3

** Calculated from weight loss after heating at 900° C

indicates a latest Miocene age (6.5 ± 0.4 Ma and 6.0 ± 0.4 Ma; Fig. 4B). The spectra are low precision and low resolution because of the small sample size and relatively young age, but the hornblende age date brackets the plagioclase date and thus supports it. The plagioclase and hornblende age determinations indicate that the stratigraphic section is of latest Miocene age. This age replaces a tentative age on unseparated plagioclase reported by Yancey and Mustoe (2007).

Details of the $^{40}Ar/^{39}Ar$ dating method are provided in Supplementary Data 1[1]. Supplemental data available for the age determination are available at the New Mexico Bureau of Geology and Mineral Resources.

SEDIMENTS OF THE LOWER WILKES FORMATION

Lithologic descriptions of depositional units, including the siderite-goethite concretion-bearing horizons, of the Lower Horseshoe Bend section are presented in Table 2 and Supplementary Data 2[1]. Strata in these sections are divisible into three intervals that record deposition in a succession of environments: (1) a lower unit of tabular mudstone beds; (2) a middle unit of lignite, volcanic ash, and tabular mudstone beds; and (3) an upper unit of concretion-bearing mudstone and thin sandstone beds. Most sediment contains a wide range of grain sizes and small or large pieces of wood. Grain size distributions of sediments made by Malvern laser diffraction and sieving of dispersed sediment often produced different grain size data (see discussion in Methods section), and grain size is reported for only a few samples.

Lower Depositional Unit

The lowest exposed sedimentary unit consists of at least 8 m of mudstone deposited in four tabular beds, each 1–3 m thick. The base of the Lower Depositional Unit is not exposed in either section. These mudstone beds have little internal layering and are roughly normally graded with thin upper layers of carbonaceous mud containing abundant wood debris (Fig. 6A). Sediments are poor to moderately sorted and consist dominantly of silty mudstone with some muddy sandstone. Dispersed wood fragments and in-place stumps or stems of trees are present in some units (Figs. 5C–D), although no fossil soils have been identified. Basal contacts show little or no indication of scour or erosion of underlying sediment, but soft-sediment deformation of underlying mud sediment occurs at a few horizons (Fig. 6A). No channels of significant size were observed in the outcrops. An upward-fining grain size of the mudstone beds is evident in comparisons of basal, mid and top layers, but little grain size variation occurs within the main body of each unit, where both upward-fining and upward-coarsening intervals occur (Fig. 6A). Most of each bed consists of sediment with a dominant mode of fine-medium silt-size particles (determined by Malvern Mastersizer laser diffraction; Fig. 6B) and a sand component of <10% (determined by wet washing and screening).

The 3.2-meter-thick bed (best exposed in the Red Gate section) is the thickest mudstone and has a complex pattern of internal bedding (Fig. 6A). The basal two meters consist of an interval of upward-fining deposits ranging from a thin layer of moderately well sorted sand at the base to crudely laminated muddy siltstone with an upper part containing large swirls of deformed sediment. This is overlain by 0.6 m of crudely bedded sediment and an upper 0.6 m of silty mudstone with many large pieces of wood in varied orientations. The disturbance features in the middle of this mudstone bed record deposition of a second pulse of high-energy flow while the underlying sediment was soft enough to be deformed by shearing from the later flow.

The top 10% or less of each mudflow unit usually contains a transitional zone of mud sediment containing irregular mud clasts (Fig. 6D) and an upper wood-rich carbonaceous clay-silt layer (Fig. 6C). This wood in the top of a bed consists mostly of branches and stems flattened by compaction and they are aligned horizontally.

Some horizons within the mudstone beds (see Fig. 3) contain many small masses of siderite. They range from 0.2 mm diameter nodules to fused aggregates of irregular shape up to 2 cm in length. Mudstone at the base of the Lower Horseshoe Bend section contains large, poorly cemented areas of sediment reaching 1 m in size, formed of aggregates of tiny prismatic bowtie siderite crystals ranging from 0.04 to 0.3 mm in length.

Middle Depositional Unit

The middle 7–8-m-thick interval contains interbedded volcaniclastic mudstone, carbonaceous clayey mudstone and lignite beds or woodmats containing large pieces of wood. These beds extend laterally across outcrops with little variation in thickness. Also present are two volcanic ash beds within lignite, one near the base and the other near the top of the interval. The contrasting colors of black lignitic sediment and white-gray mudstone and white volcanic ash make this interval conspicuous in streambank exposures. The mudstone beds are thinner and finer grained than mudstone beds of the lower interval and are overlain by thick wood-rich lignites or woodmats. Woodmats are the most distinctive component of this interval (Fig. 5A), being composed of stems and logs that are only partially carbonized. Thicker pieces of wood often retain a light brown coloration similar to fresh wood (Fig. 5B). Roberts (1958) noted this type of wood preservation in the Wilkes Formation and Mullineaux et al. (1959) reported similar woody material in the upper Miocene nonmarine deposits farther north in the Puget lowlands. The mats of horizontal wood pieces are more resistant to erosion than other sediments and erode out in relief on slopes, tending to hold together and produce large blocks that slide down the bluff to creek level.

The two volcanic ash beds have variable thickness within the enclosing carbonaceous sediment. The lower ash bed in the Lower Horseshoe Bend section (Figs. 5E–F) is 10–20 cm thick and contains fragments of wood within the ash. The upper ash has a finer grain size than the lower ash and the bed is discontinuous or not recognizable in some places. Both volcanic ash beds contain large (to 1 by 5 mm) authigenic vermiform crystals of kaolinite.

Upper Depositional Unit

The upper 6-m-thick interval contains mudstone and sandstone in poorly defined beds that have limited lateral extent in outcrop. The top of the unit is formed by an erosion surface. The sediment is dominantly

[1] palaios.ku.edu

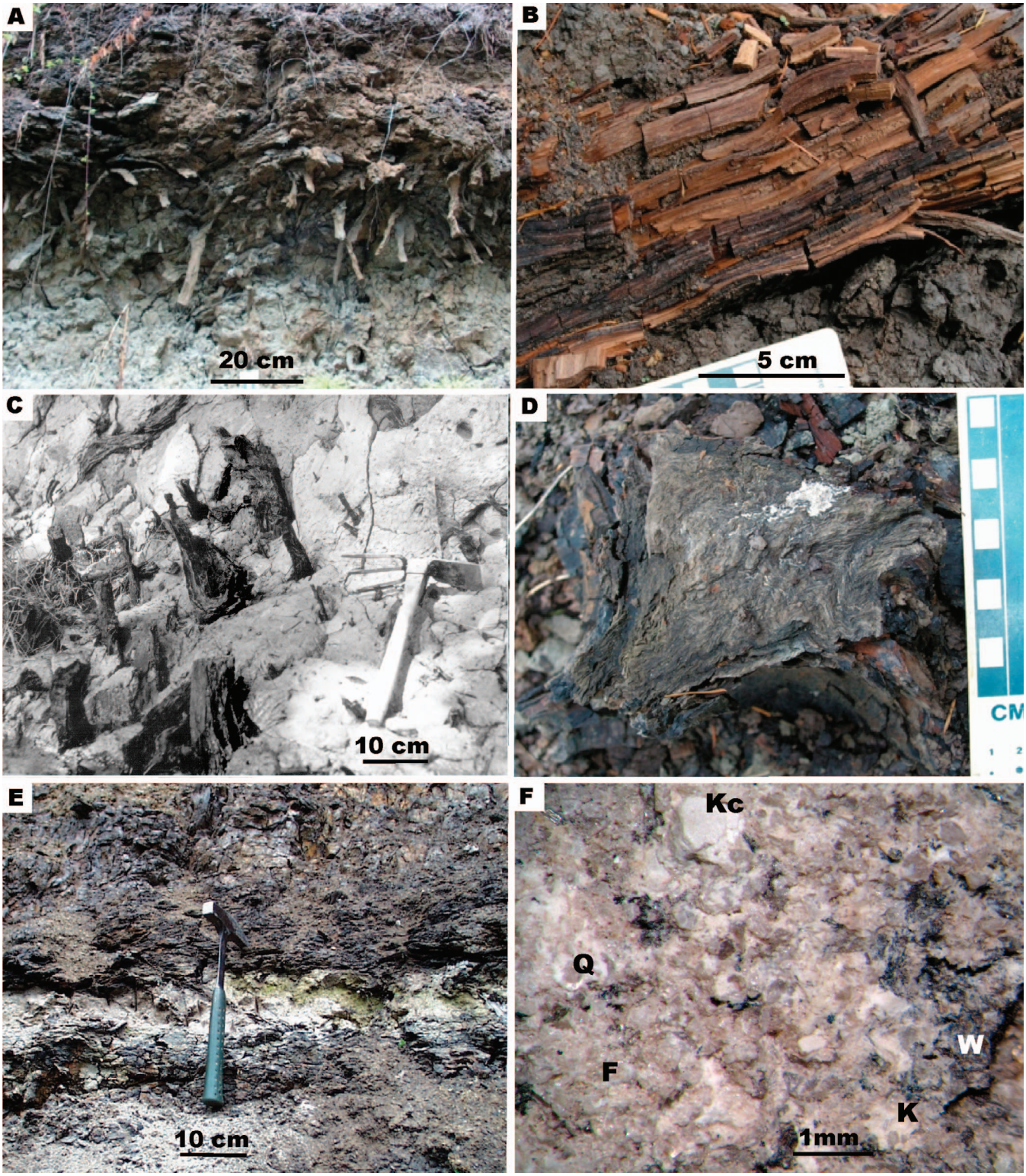

FIGURE 5—Plant remains and volcanic ash beds in Lower Horseshoe Bend section, WWU 1571. A) Woodmat at the top of the middle unit with flattened stems and trunks bent downward after enclosing sediment is removed by erosion. B) Large piece of trunk wood in lower lignite in middle unit, showing effects of desiccation but little carbonization. C) Group of stumps exposed in the lower part of flow unit #2 at edge of Salmon Creek (photo used in Mustoe, 2001). D) Vertical downward view of stump with buttress roots exposed, in the lower part of flow unit #3. E) Lower volcanic ash bed, occurring as a tonstein in lignite bed. F) Photo of lower volcanic ash, showing quartz (=Q) and feldspar (=F) phenocrysts and kaolinite as large authigenic vermiform crystals (=Kc) and matrix (=K) and larger carbonized wood fragment (=W). Vermiform kaolinite crystals are common in these volcanic ash beds.

silty to sandy mudstone, with muddy sand layers (to 30 cm thick) most abundant in the middle of the unit (Figs. 7A–B). When exposed, the clay content of these sediments causes them to crack into irregularly shaped small blocks, producing recessive, colluvium-mantled slopes. Mudstone beds are not laminated and they contain common small to very small pieces (stems and branches) of wood in random orientation (Fig. 7B). Most mudstone is very poorly sorted with a wide range of grain size from clay to fine-grained sand. Beds of sandstone are poor to

TABLE 2—Summary of lithofacies in the lower Wilkes Formation, Lewis County, Washington.

Sediment type	Lithology	Bedding	Sedimentary structures	Fossils	Concretions	Depositional environment	Depositional unit
Sandstone	Moderately sorted sand with mud matrix	Minor lamination and sharp basal contact; to 10 cm thick	Upward-fining size trend	Small wood pieces	None observed	Flowing water	Upper; lower
Mudstone (silty)	Silt-rich mixture with sparse sand	Thick bedded, sharp basal contacts; swirled bedding in some	Upward-fining size trend	Stumps in growth position, large wood pieces	Minute bowtie siderite; porous masses of bowtie siderite	Volcanic mudflow	Middle; lower
Mudstone (clayey)	Clay-silt mixture with minor sand	Massive, no lamination	None observed	Common small wood pieces	Abundant elongate and irregular siderite; common minute bowtie siderite	Standing water of lake of ponds	Upper
Mudstone (carbonaceous)	Clay mud with plant pieces	Medium bedded, gradational contacts	None visible	Wood pieces	None observed	Swamp	Middle
Lignite	Wood and plant detritus with minor clay mud	Layering of wood pieces	Compaction of wood	Wood	None	Swamp	Middle
Volcanic ash	Broken crystals in kaolinite matrix; vermiform kaolinite	Thin and variable	Massive	Wood pieces (in lower)	None	Swamp	Middle

moderately sorted, have vague lamination, and tend to have sharp basal contact and gradational upper contact with mudstone. Even the better-sorted sandstone layers have mud matrix between the grains. Sand grain composition is more varied than the sand fraction of mudflow deposits, containing nonvolcanic grains such as chert and sand-sized grains of mudstone in addition to volcanic phenocrysts and volcanic rock fragments. Rounding and polishing is present on some larger grains. Beds of sand contain some small burrows with poorly defined walls.

Siderite concretions with a wide range of size and form are common in the upper 3 m of this unit, occurring within mud-rich sediment. All concretions collected *in situ* in the unit have siderite-goethite composition. Many concretions occur as coprolite-shaped sinuous or elongate masses with tapering ends (Figs. 7C, E). The more sinuous concretions often have a cracked, breadcrustlike surface (Fig. 7E). More common are concretions with a vague sinuous form and irregular surfaces variably covered with small nodes (Figs. 7C–D). Node attachment ranges from weakly attached spheres to hemispheres to groups of merged nodes forming a composite mass of large cauliflower shape. Surfaces of the siderite concretions are oxidized and have rinds of goethite. Concretions composed entirely of goethite (Figs. 7D, 8E–F, 9) occur loose in the steam bed of Salmon Creek or in Pleistocene terrace deposits, but none were found *in situ* in Wilkes Formation sediments. The iron oxides of these concretions were formed by oxidation alteration of siderite, as shown by concretions with varying stages of siderite replacement (Fig. 8E). Also present in the sediments are abundant tiny (0.03–0.1 mm) prismatic siderite crystals; many with flared terminations that produce a bowtie morphology (Fig. 10). These minute crystals occur in many horizons of clay-rich sediment around siderite concretions, in mudstone, and in sand-dominated sediment layers.

INTERPRETATION OF DEPOSITIONAL ENVIRONMENTS

The volcaniclastic mudstone beds of the lower and middle depositional units are interpreted to be mudflow deposits related to volcanic activity. A volcanic origin for the sediment is indicated by the abundance of angular lithic clasts and presence of euhedral (including clear bipyramidal quartz crystals) and angular fragmental phenocrysts in the sand fraction. Particle size distributions of mudstone and reworked sediment (Fig. 11) resemble sediments of modern distal lahar and lahar runout mudflow deposits (Scott, 1988). The high proportion of silt-sized grains in the sand-silt-clay fraction of these deposits contrasts with the grain size characteristics of nonvolcanic flows (Fisher and Schmincke, 1984). The Wilkes Formation sediments commonly have a primary mode in the very-fine silt size range (2–4 μm; Fig. 6B). The small grain size of the sediment and weak bedding indicates deposition from hyperconcentrated flow, with the finer-grained top layers of each cycle produced by mud expelled during settling of the deposit (Pierson, 2005). The better sorted basal sand of the 3.2-meter-thick mudstone probably represents more dilute portions of the flow, but there is little indication of basal scour or erosion, so this is interpreted to be deposited by sheet flow spreading out from a channel. The presence of tree stems preserved in upright position (Figs. 5C–D) indicates sufficient time between events for trees to grow on the tops of mudflow beds. Mustoe (2001) also records in-place stumps in these deposits. Similar deposits have been observed in the local area as a result of eruptions of Mount Saint Helens during 1849–1850 and 1980 (Karowe and Jefferson, 1987; Yamaguchi and Hoblitt, 1995).

The concentration of low-density wood particles at the top of mudflow deposits is compatible with deposition of suspended organic debris during the last phases of flow accumulation. In the 3.2-meter-thick mudstone unit, the wood particle-rich layer is underlain by a thin mud-clast-rich layer containing light-colored clay-rich clasts with irregular outlines that probably had high water content at the time of deposition. These layers are interpreted to have been deposited last, during the waning stages of mudflow. The larger size of some mud clasts and wood particles makes it improbable that they were expelled from the main body of the mudflow. Our interpretation is that these larger components were either present in a lower-density surface layer of the flow or settled out from a late-stage, lower-density part of the flow.

Beds of carbonaceous mudstone, lignite-woodmat and the two ash fall beds extend laterally across outcrops with little evidence of disturbance by high-energy currents, indicating deposition in quiet water conditions. The lack of lamination suggests that the sediment remained fluidized after deposition and/or that small invertebrates churned the sediment. The lignites could have accumulated as peats beneath a canopy of living trees, but the dominance of coarse wood fragments in the lignite suggests the possibility of accumulation due to

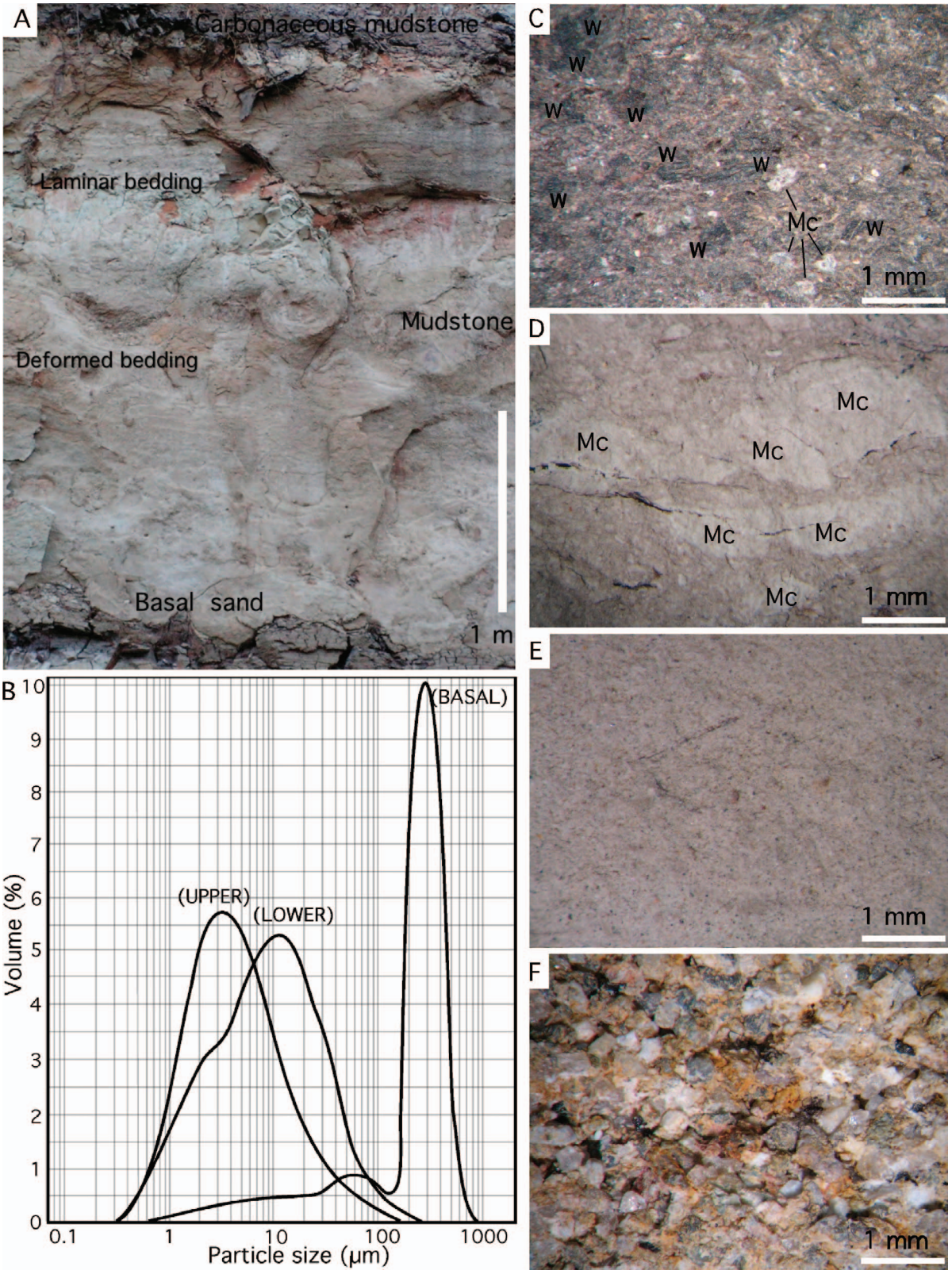

FIGURE 6—Volcanic mudstone flow units in Red Gate section, WWU 2138. A) Flow unit #3 showing an upward-fining grain size trend and different layers within the flow unit. Irregularities on the basal surface result from differential deformation of underlying sediment. Circular structures in the middle of the flow result from internal deformation of moving sediment. B) Representative sediment grain size distribution (Malvern laser spectrometry) of samples within a flow unit. C) Bedding plane view of plant scrap–rich unit at top of flow unit containing low-density particles (mostly wood, =W) and small mud clasts (=Mc, white). D) Bedding plane view of mud clast-rich layer below capping plant-rich layer with white mud clasts (=Mc) set in tan-colored mudstone matrix. Irregular outline of mud clasts suggests tearing and fragmentation during transport. E) Silt-rich mudstone from middle of flow unit, with dispersed sand-sized grains visible. F) Sand layer at base of flow unit with dominant mode of medium-size sand grains.

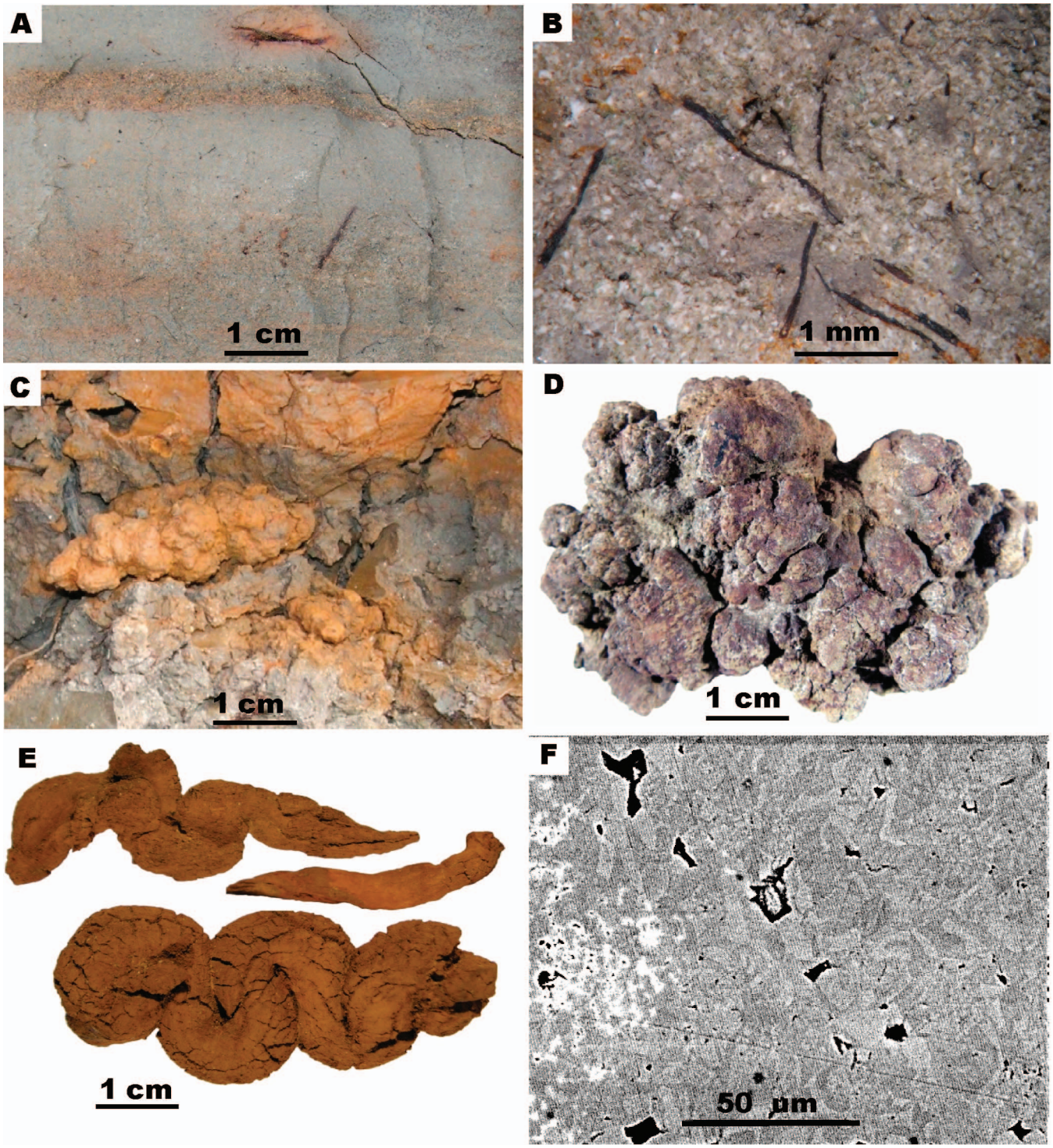

FIGURE 7—Sediments and concretions of the upper depositional unit in Lower Horseshoe Bend section WWU 1571. A) Sand layers in clayey mudstone. Sample from 12.5 m above base of section. B) Example of grain-rich mudstone with common small-diameter wood fragments and mudstone clasts (gray masses). Sample from 12.8 m above base of section. C) Irregular-noded siderite concretion with iron oxide rind and tapered ends. *In situ* sample from 15.6 m above base of section. TAMU Wilkes sample #12. D) Top surface of flattened irregular concretion with many attached nodes. 15.6 m above base of section. TAMU Wilkes sample #14. E) Semi-irregular siderite concretions with tapered ends, fine longitudinal striations on surface between nodes and breadcrust cracking. Samples from top of section. TAMU Wilkes samples #22, #23 and #27. F) Backscattered electron (BSE) image of equant-sized siderite crystals (gray) in siderite concretion. White areas are masses of iron oxide and black areas are small cavities in concretion. Sample from 15.6 m above base of section. TAMU Wilkes sample #18.

sinking of logs floating in wood rafts derived from wood-logs transported into the basin by mudflows. Extensive log rafts present on the newly created Coldwater and Castle lakes in the Toutle Valley after the 1980 Mount Saint Helens eruption are a modern analog (Dahm et al., 2005).

The upper ash bed is discontinuous or not recognizable in some places, but this appears to be due to local, limited disturbance soon after deposition. The lower ash bed in the Lower Horseshoe Bend section (Figs. 5E–F) is 10–20 cm thick and contains fragments of wood, indicating that airborne ash settled onto a wood-covered substrate or

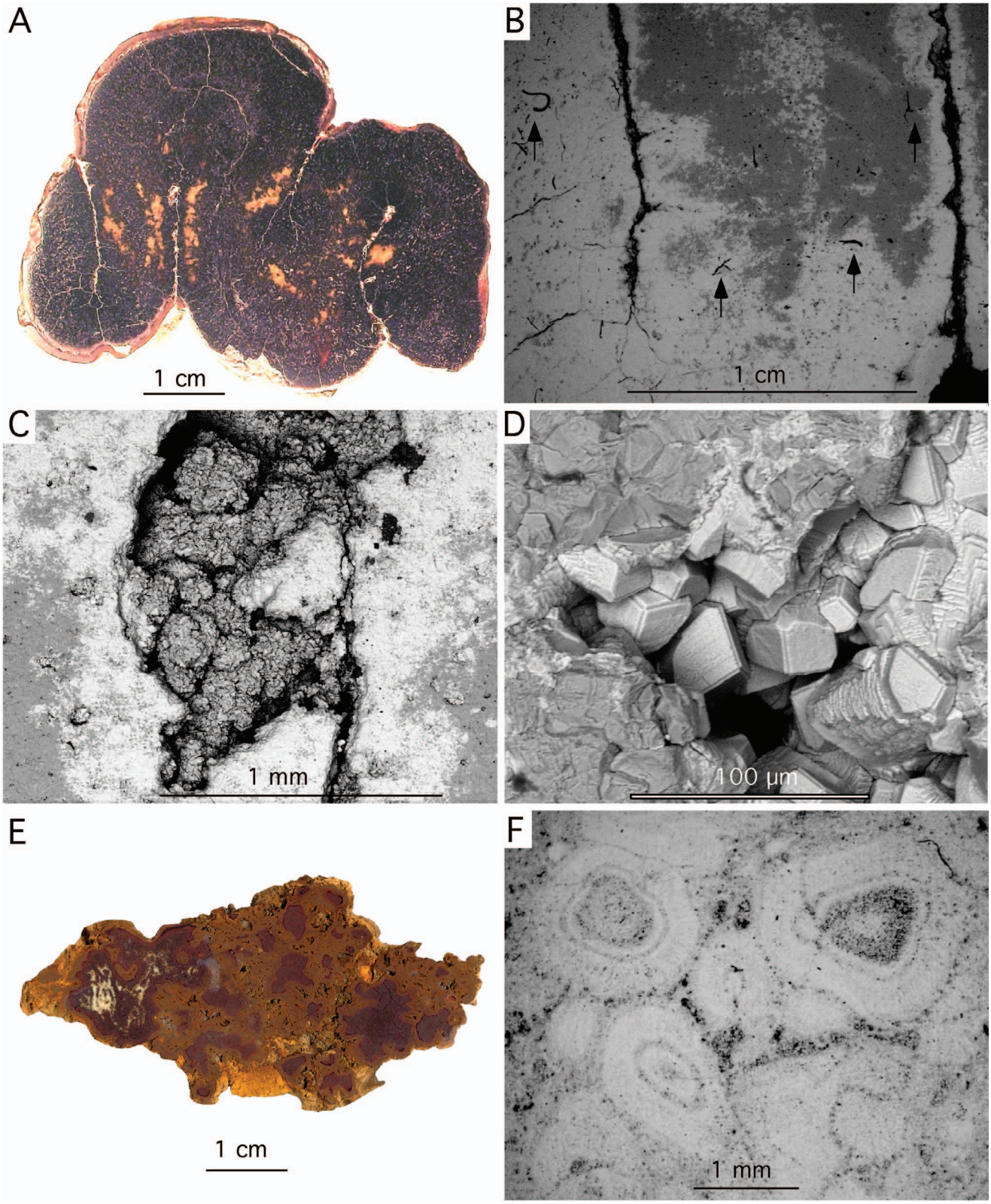

FIGURE 8—Alteration of siderite concretions by iron oxides. A) Sinuous concretion with remnant siderite in interior (white) and replacement goethite (brown). WWU Wilkes concretion #4. B) BSE image detail of cut surface of interior showing surface to interior progression of goethite (white) replacement of siderite (gray) and small curved inclusions (arrows) of probable organic matter. In this BSE image siderite appears as dark in contrast to light-colored in white-light photograph. WWU Wilkes concretion #4. C) BSE image of clusters of siderite crystals grown in void on side of coil of sinuous concretion. WWU Wilkes concretion #4. D) Euhedral siderite crystals with thin surface crust of goethite (white) filling void in concretion. WWU Wilkes concretion #2. E) Very altered concretion with a small remnant of siderite (white, on left side), surrounded by replacement goethite (dark brown) and other iron oxides (light yellow brown) in irregular domains. WWU Wilkes concretion #6. F) Very altered concretion with orbicular domains of iron oxide replacement indicative of chemical diffusion from surface to interior of domains. WWU Wilkes concretion #3.

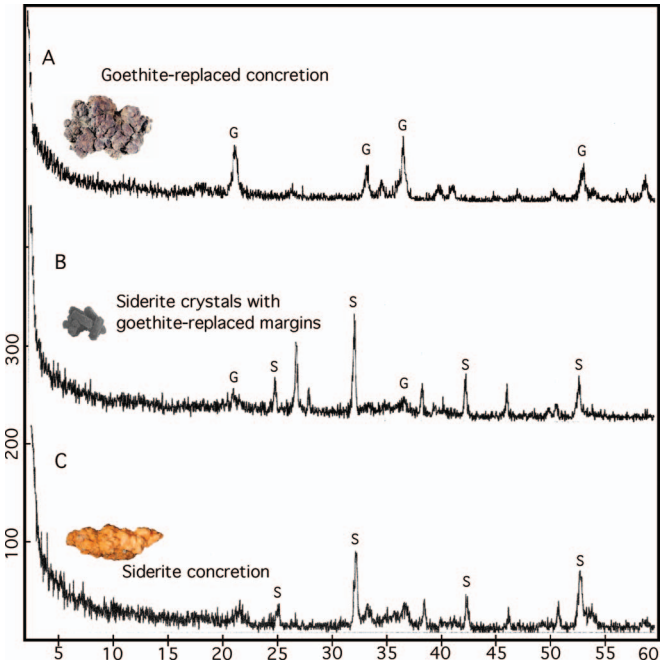

FIGURE 9—X-ray diffraction records of concretions and prismatic siderite crystals in sediments of the Wilkes Formation in Lower Horseshoe Bend section WWU 1571. A) Elongate concretion with tapered ends replaced with goethite (iron oxide). Displaced concretion collected from stream bed. TAMU Wilkes sample #7; photo of concretion from 15.6 m above base of section, TAMU Wilkes sample #12. B) Bowtie prismatic siderite crystals with siderite core and goethite margins. Goethite is dominant by volume but is poorly crystallized, so the siderite component dominates the X-ray pattern. Sample from 17.2 m above base of section; photo of crystal cluster from 0.01 m above base of section. C) Irregulary concretion replaced with goethite (iron oxide). 15.6 m above base of section. TAMU Wilkes specimen #14.

that pieces of waterlogged wood settled along with the volcanic ash particles.

Upper unit sediments show no evidence of subaerial exposure or soil development during deposition and no sphaerosiderite nodules indicative of soil zones was recognized in Wilkes Formation sediments. Laterally impersistent bedding occurs at both large and small scale, and poor sediment sorting suggests deposition in normally quiet waters of lakes, with intermittent variations in current flow. The presence of a mixed water-transported and air-transported pollen assemblage (see discussion in following section) supports the interpretation of deposition in standing water. The presence of thin layers of fine sand provides evidence of current deposition, but the scarcity of well-sorted sand rules out sustained current action or persistent wave activity. The absence of lamination, presence of only a few burrows, and presence of wood in nearly random orientation in muddy sediment points to stirring of bottom sediments after deposition, although later postdepositional disturbance by concretion growth has contributed to obliteration of small bedding features.

POLLEN ASSEMBLAGES

Sediments of the Wilkes Formation contain plant fossils and well-preserved pollen, providing a record of plant assemblages in the area of deposition and additional data on depositional environments. Strata in the study area contain both transported wood fragments and upright stems and trunks buried *in situ*. Although leaf fossils provided an age determination of the Wilkes Formation (Roberts, 1958), pollen provides a detailed record of the palynoflora within the lower Wilkes Formation (Leopold et al., 2007; G. E. Mustoe and E. B. Leopold, personal communication, 2013). Diverse assemblages of well-preserved pollen and spores are present in sediment samples from the middle and upper depositional units of the Lower Horseshoe Bend section (Fig. 12), supplemented with a sample from nearby exposures of the concretion-bearing part of the upper unit.

The middle depositional unit, with several lignite beds or woodmat beds, contains a *Nyssa* (tupelo)- or *Taxodium* (cypress)-dominated pollen assemblage typical of plants living in swamp or lake-margin settings (McWilliams et al., 1998). One sample (SC-4) contains a high amount of algal cysts in the pollen assemblage and a different sample from a nearby site (not shown in Fig. 12) contains *Nymphaea* (waterlily) pollen, indicators of standing water conditions. Two of the lowest samples (SC-1 and SC-3) contain notable occurrences of the pollen of *Nyssa* in addition to *Taxodium*, trees that are dominant in swamps similar to the modern *Taxodium distichum–Nyssa aquatica* swamp forests of southeastern North America (McWilliams et al., 1998). The overlying sample SC-4 and samples from the upper part of the middle unit and basal part of the upper unit (SC-7–SC-10) contain a *Taxodium*-dominated assemblage with minimal amounts of *Nyssa* (Fig. 12). The highest sample (SC-12) has a pine-dominated assemblage and lacks *Nyssa* entirely.

Located between the lower *Taxodium*/*Nyssa*-dominated and higher *Taxodium*-dominated swamp assemblages are two pollen samples with less indication of swamp deposition. The lower sample (SC-5) contains a majority of fern spores, an assemblage that is typical of deposition under conditions of environmental disturbance and loss of vegetation cover, and the upper sample (SC-6) has a mixed forest assemblage of mixed gymnosperm and angiosperm pollen and low levels of *Taxodium* pollen. This mixed forest assemblage comes from mudstone sediments and the pollen was probably transported from outside the immediate area rather than being produced by plants living at or beside the site of deposition.

Pollen samples from the concretion-bearing portion of the upper depositional unit contain an abundance of hardwoods and gymnosperms typical of dryland settings (samples SC-11, CO-1). These samples contain more pine and *Alnus* (alder) pollen than underlying samples and have the highest levels of *Pterocarya* (wingnut) and *Juglans* (walnut) pollen present in the section (Fig. 12). These upper level pollen assemblages are interpreted to be a composite of water-transported and wind-transported grains, representing a mixed forest assemblage deposited in open water.

Pollen assemblage trends indicate a long-term change from a *Taxodium*/*Nyssa*-dominated assemblage in the lowest samples to a *Taxodium*-dominated assemblage in higher samples and continued change to an assemblage with transported *Pterocarya*/*Juglans* in the highest samples. These palynological changes parallel sediment depositional change from deposition on forested lowlands to deposition in swamp–lake-margin environment to deposition in standing water environment.

DISCUSSION

The uppermost Miocene section of the Wilkes Formation provides new data on the geologic development of the southern Puget lowlands during a time of tectonic change and climate change. The lower Wilkes Formation records a time of active volcanism when volcanoes produced large mudflows spreading onto forested lowland, similar to the volcanic activity of andesitic volcanoes located in the area today. Mudflows in the two described sections have tabular form and similar thicknesses at locations a half kilometer apart, indicating large volume flows spreading onto a flatland surface. The presence of preserved tree stumps in the mudflows fits with this interpretation of flows spreading onto broad valley bottomlands at some distance from the sides of volcanoes.

The middle part of the section contains a series of deposits from swamp environments interbedded with thinner mudflows and the upper part of the section contains standing water deposits of lacustrine

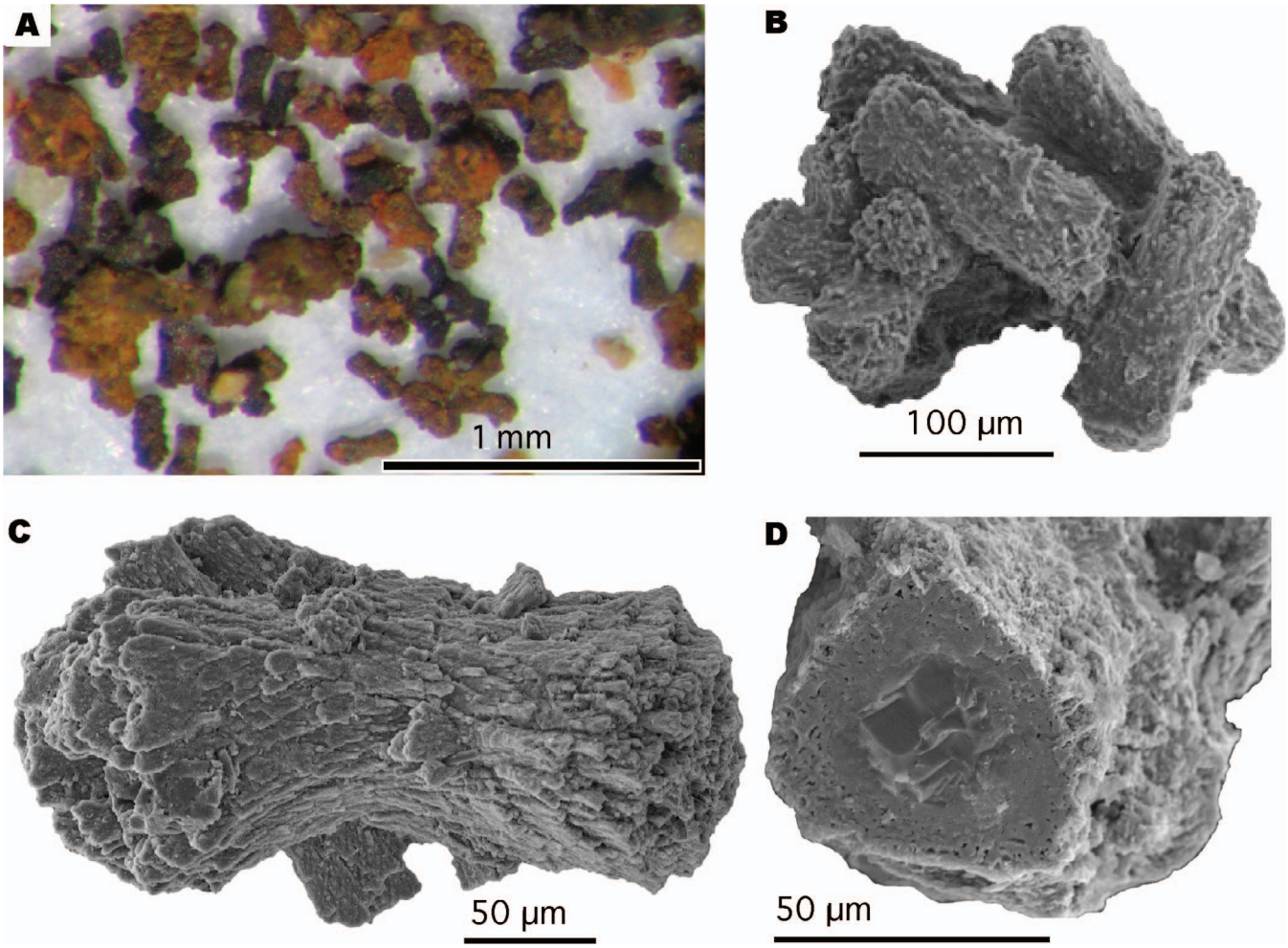

FIGURE 10—Siderite bowtie prism crystals in Lower Horseshoe Bend section WWU 1571. A) Bowtie prism crystals and small concretionary aggregates of siderite crystals in silty mudflow sediment. Aggregates are formed of crystals fused into clusters and weakly cemented sediment between crystals. Sample from 0.01 m above base of section. B) Fused aggregate of crystals. Sample from 0.01 m above base of section. C) Single crystal showing characteristic flaring on ends of prism. Sample from 15.6 m above base of section in sediments adjacent to large siderite concretion. D) Cross section of siderite bowtie prism showing larger crystal unit in center and irregular microcrystalline goethite on outer portions, containing small voids near surface. Sample from 15.6 m above base of section in sediments adjacent to large siderite concretion.

depositional environments. This part of the section records rising water levels and corresponding rise in base level for the basin. The lake deposits of the upper part of the section contain common siderite concretions over a distance of ~10 km along Salmon Creek, indicating the presence of a lake or interconnected series of ponds and lakes in the basin. The subdominant presence of pollen from wind-pollinated plants adapted to dryland environments suggests a lake environment, because the more open expanse of a lake provides a greater opportunity for wind-transported pollen to accumulate than in the more closed and tree canopy-protected settings of ponds and swamps. With the presence of active volcanoes in the area, the lake basin could have been formed by either tectonic means (dropping the basin or raising a barrier to drainage) or by eruptive activity that built a barrier to water flow in the drainage basin. The size and extent of this lake basin remain to be determined.

Paleobotanical evidence provides a good determination of climate conditions in the southern Puget lowlands at the end of the Miocene. The occurrence of a *Taxodium*/*Nyssa*-dominated swamp assemblage indicates the lower Wilkes Formation was deposited during a time of warm, summer-wet climate (McWilliams et al., 1998). It is the youngest known occurrence of *Taxodium* swamp flora in the Pacific Northwest. The Wilkes Formation contains the only upper Miocene locality west of the Cascade Crest in Washington with documented leaf fossils and fossil pollen (G.E. Mustoe and E.B. Leopold, personal communication, 2013), providing an opportunity to compare leaf floras and pollen assemblages on opposite sides of the Cascades during a time of Cascades uplift. Late Neogene climate change of the Pacific Northwest is a record of cooling of mean annual temperatures from Miocene summer-wet climates combined with a northward spread of summer-dry climates in the interior region distant from coastal moisture (Wolfe and Hopkins, 1967; Wolfe, 1987). The uplift of the Cascades in central Washington and Oregon produced a well-developed rain shadow (Chaney, 1948; Smiley, 1963; Wolfe, 1987) that strengthened the trend of interior drying. Summer-dry climates were present in the interior during the early Pliocene, followed by an interval of relatively stable wetter climate developed over the western states from 3.5 to 2.5 Ma (late Pliocene) that allowed large persistent lakes to develop (Forester, 1991). A return to summer-dry climates occurred during further cooling associated with the advent of glaciation during the Pleistocene. Timing of the uplift and development of an obvious rain shadow in central Washington is based on tectonic and paleobotanical work (Smiley, 1963; Leopold and Denton, 1987; Reiners et al., 2002; Cheney and Hayman, 2007) calibrated with geochronologic dating (Smith, 1988; Smith et al., 1988).

Siderite formed within Wilkes Formation sediments at several levels, forming solid, crystalline siderite concretions within clay-rich lakebed sediments (Figs. 7C–F) and as tiny prismatic crystals (rarely over 0.2 mm in length) with bowtie morphology scattered through the sediment at

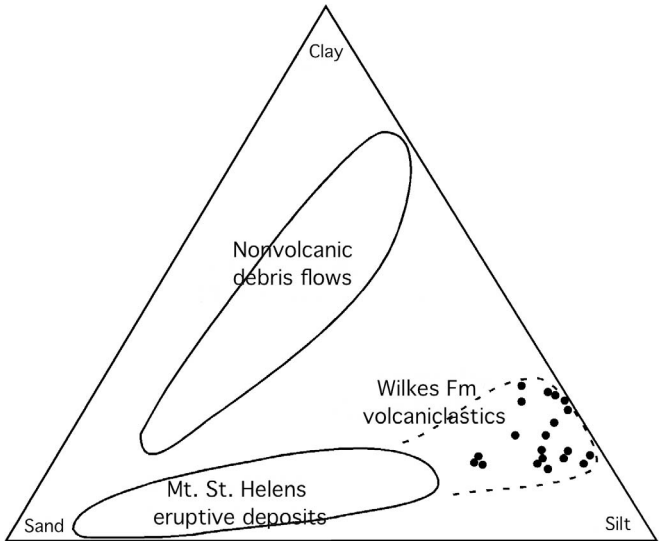

FIGURE 11—Particle size distributions of sand-silt-clay fraction of Wilkes Formation volcaniclastics (black dots within field indicated by dashed line) compared with fine fractions of Mt. St. Helen eruptives and nonvolcanic flow deposits, illustrating high proportion of silt particles in Wilkes Formation deposits. Grain size fields of nonvolcanic debris flows and Mt. St. Helens eruptives taken from Fisher and Schmincke (1984). Wilkes Formation data based on Malvern laser diffraction analysis of 18 samples collected for this study.

many levels (Fig. 10). These tiny prismatic crystals occur in sand-bearing sediments with a fine clay-rich matrix and in the matrix around most large siderite concretions. They have an elongate prism form, although most have slight to strong flaring terminations (Figs. 10A, C) and they have a rough outer surface (Fig. 10C). The crystals are often fused together in jackstraw clusters (Fig. 10B) and where abundant they are intergrown into large spongy masses with sediment remaining between crystals. These cement the sediment into semiconsolidated masses with diffuse margins that are atypical of other concretions.

The prisms have a coarsely crystalline core and a thick microcrystalline outer rim (Fig. 10D), and bulk powders of the prismatic crystals produce an X-ray diffraction pattern corresponding to siderite composition with a small component of goethite present (Fig. 9B). Microprobe EDS analysis reveals a pure siderite composition for the core and an iron oxide (goethite) composition for the microcrystalline rim, indicating the rims are alteration products of siderite. The amount of remnant core varies and some prisms have little to no siderite present. Although goethite is volumetrically dominant in the prisms, X-ray powder diffraction patterns are dominated by strong sharp reflections from the coarser crystalline siderite. In these samples goethite gives a weak signal of its presence. This unequal X-ray response is expected in mixtures of coarsely crystalline and poorly crystalline minerals (R. Guillemette, Texas A&M University, personal communication, 2012).

Some Wilkes Formation concretions have features that obscure an understanding of their origin. Most concretions collected from the streambed of Salmon Creek or in Pleistocene terrace deposits are altered by weathering. Oxidation alteration of the concretion siderite proceeds inward by chemical diffusion from outer surfaces or cracks propagating within the interior, producing an irregular pattern of remnant masses of siderite surrounded by iron oxides (Figs. 8A–B). Subsequent alteration of goethite may produce goethite remnants surrounded by porous mixtures of iron oxyhydroxides (Fig. 8E), recognized by their yellow-brown coloration. Strongly altered concretions may show concentric diffusion bands and an orbicular fabric (Fig. 8F).

Siderite concretions in the upper depositional unit are composed of solid intergrowths of siderite crystals (Fig. 7F) with a composition of >99 mol% $FeCO_3$ (WDS microprobe analysis). This is characteristic of siderite precipitated in low-sulfate fresh-water environments (Mozley, 1989) and is compatible with an origin primarily by replacement of sediment (Fisher et al., 1998) in contrast to cementation of sediment. These large siderite concretions contain few or no inclusions of other material. The lack of inclusions is a typical microstructure for early formed siderite concretions that grow by simultaneous nucleation across the entire concretion mass (Fisher et al., 1998), a process associated with microbially mediated siderite precipitation in materials close to the sediment-water interface in the methanogenesis burial zone. The noded siderite concretions appear to be composites of elongate forms and small spheres that formed simultaneously in adjacent sediment and grew together. The less-noded concretions (Fig. 7E) tend to have a breadcrust cracking of the outer surface, indicating an increase in volume during mineral replacement or shrinkage due to water loss from the original material. The most irregular concretions are completely replaced with goethite (Fig. 7D).

The presence of decaying vegetation and organic-rich waste in sediments of a fresh-water environment provides the chemical conditions needed for rapid replacement of bacterially decomposing organic matter. Duan et al. (1996) report rapid growth of siderite concretions in modern organic-rich sediment, aided by the growth of iron-reducing bacteria. Mustoe (2001) concluded that Wilkes Formation siderite nucleated and grew during the early stages of diagenesis in the sediments, a timing that is consistent with preservation of extrusional surface fabric and the bacterial-aided precipitation of siderite. Carbon isotope values of Wilkes Formation siderite ranges from −11‰ to −13‰ (Mustoe, 2001), indicating siderite precipitation within the methanogenesis burial zone, not in an area of methane seepage and oxidation near the sediment-water interface (Hicks et al., 1996).

The controversy about nonbiogenic versus biogenic fecal origin of coprolite-shaped concretions remains unresolved. The twisted morphology of unoxidized siderite concretions with surface striations indicates a starting condition as an extruded soft paste and their environmental occurrence in anoxic mud-rich lakebed sediments is compatible with a fecal origin for the extruded paste. However, evidence of identifiable food remnants (seeds, tissue, or skeletal remains) in the concretions is minimal (Fig. 8B) and indeterminant. A chemically induced breakdown of hard organics during siderite precipitation in the paste is possible, but identification of chemical processes capable of both weakening and dispersing refractory organic material (such as lignin) is needed for accepting a fecal origin for the concretions.

CONCLUSIONS

Sedimentary strata of the lower Wilkes Formation exposed in the banks of Salmon Creek provide a record of inundation of latest Miocene forested wetlands in the Puget lowlands west of the Cascade Range. The lowest beds record deposition of multiple volcanic mudflows into the area and continued deposition under conditions of rising water levels, changing to swamp and smaller volcanic mudflows and culminating in standing water lake deposits. Aquatic deposits contain a record of progressive change in local vegetation cover that corresponds with environmental change recorded by the sediments. Large amounts of wood debris are preserved in mudflows and in lake deposits as well as in swamp deposits and lignite-woodmats. Larger pieces of wood in woodmats are not completely carbonized, preserving fresh-appearing areas of wood in their interior. The only indication of subaerial exposure for sediments present in the section is the presence of tree stumps in growth position on the tops of volcanic mudflows. Mudflows were deposited by flowing mud-water mixtures and all other sedimentary units indicate deposition in standing water.

The lowest lignites contain pollen of a *Taxodium*/*Nyssa* swamp assemblage, followed by deposition of a *Taxodium* swamp assemblage and later by deposition of a mixed forest assemblage of water- and wind-transported pollen in an open-water environment. The Wilkes

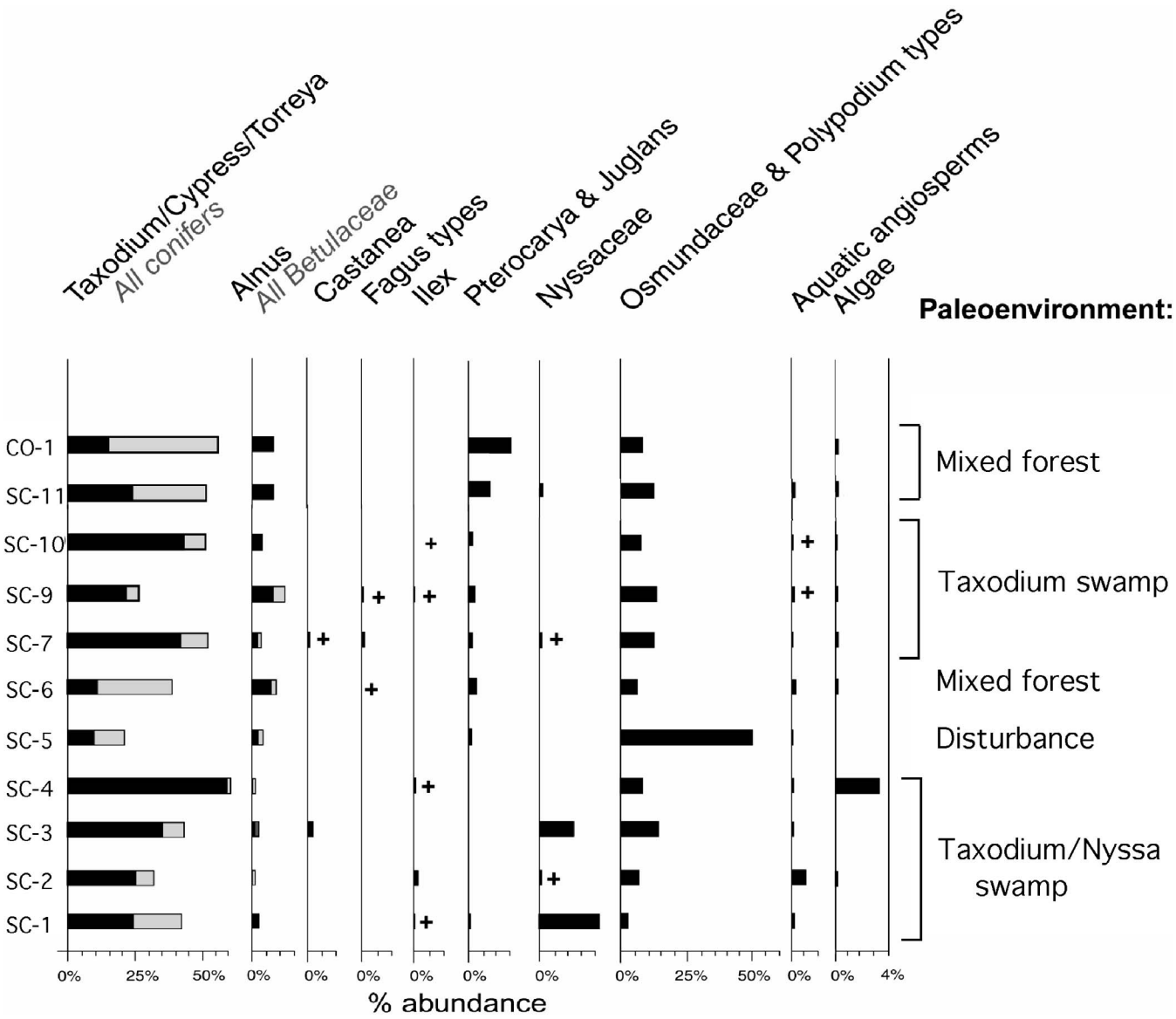

FIGURE 12—Abundances of important pollen taxa in Wilkes Formation deposits in Lower Horseshoe Bend section WWU 1571. The change from TCT (*Taxodium*) and *Nyssa* dominance to a mixed composition (indicated by *Pterocarya* and *Juglans* and *Alnus*) corresponds with a pronounced change in environment of deposition.

Formation documents the presence of a warm, summer-wet climate west of the Cascade Range during the latest Miocene, in an area of high rainfall. This contrasts with the developing summer-dry conditions in eastern Washington in response to rain-shadow effects of the Cascades volcanic chain.

Siderite concretions and tiny bowtie-shaped siderite crystals occur at many levels in Wilkes Formation sediments exposed in the study area, but coprolite-shaped concretions are limited to lakebed sediments and formed by replacement of paste materials, probably aided by bacterial growth in the source material. Siderite formed both as dense siderite replacement concretions and as small mm-scale crystals that aggregated together to form spongy masses in some layers. Siderite concretions have varying amounts of goethite alteration.

ACKNOWLEDGMENTS

Elaine Mustoe and Lew Landers participated in initial Salmon Creek fieldwork, and the senior author is especially grateful to Lew Landers for stimulating lasting interest in this unusual occurrence of concretions and the problem of trying to understand the origin of concretion formation of extrusional masses. Zha Zhongjun processed sediment samples and Linda Reinink-Smith photographed palynomorphs and made pollen counts at Estella Leopold's University of Washington laboratory. Dr. Vaughn Bryant of the palynology laboratory at Texas A&M University extracted pollen from several sediment samples. Mineral determination by X-ray diffraction determination is by A. Ferreiro, Texas A&M University, and microprobe analysis of siderite composition is by R. Guillemette, Texas A&M Microprobe Lab, in addition to work at Western Washington State University. SEM images were produced at Western Washington University and by Dr. Mike Pendleton of the Microscopy and Imaging Center, Texas A&M University. Dr. Paul Comet provided guidance on organic geochemistry. The authors thank all of these colleagues for their contributions.

REFERENCES

Amstutz, G.C., 1958, Coprolites: A review of the literature and a study of specimens from southern Washington: Journal of Sedimentary Petrology, v. 28, p. 498–508.

Chaney, R.W., 1948, The Ancient Forests of Oregon: Condon Lectures, Oregon State System of Higher Education, Eugene, Oregon, 56 p.

Cheney, E.S., and Hayman, N.W., 2007, Regional Tertiary sequence stratigraphy and structure on the eastern flank of the central Cascade Range, Washington: Geological Society of America Field Guide 9, Boulder, Colorado, p. 179–208.

Clarke, F.W., 1924, The data of geochemistry, 5th edition: United States Geological Survey Bulletin 770, 841 p.

Dahm, C.N., Larson, D.W., Petersen, R.R., and Wissmar, R.C., 2005, Response and recovery of lakes, *in* Dale, V.H., Swanson, F.J., and Crisafulli, C.M., eds., Ecological Responses to the 1980 Eruption of Mount St. Helens: Springer, New York, p. 255–274, doi: 10.1007/0-387-28150-9_18.

Duan, W.M., Hedrick, D.B., Pye, K., Coleman, M.L., and White, D.C., 1996, A preliminary study of the geochemical and microbiological characteristics of modern sedimentary concretions: Limnology and Oceanography, v. 41, p. 1404–1414.

Fisher, Q.J., Raiswell, R., and Marshall, J.D., 1998, Siderite concretions from nonmarine shales (Westphalian A) of the Pennines, England: Controls on their growth and composition: Journal of Sedimentary Research, v. 68, p. 1034–1045.

Fisher, R.V., and Schmincke, H.M., 1984, Pyroclastic Rocks: Springer-Verlag, Berlin, 472 p.

Forester, R.M, 1991, Pliocene-climate history of the western United States derived from lacustrine ostracodes: Quaternary Science Reviews, v. 10, p. 133–146.

Hicks, K.S., Compton, J.S., McCracken, S., and Vecsei, A., 1996, Origin of diagenetic carbonate minerals recovered from the New Jersey continental shelf: Proceedings of the Ocean Drilling Program, Scientific Results, v. 150, p. 311–328.

Karowe, A.L., and Jefferson, T.H., 1987, Burial of trees by eruptions of Mount St. Helens, Washington: Implications for the interpretation of fossil forests: Geological Magazine, v. 124, p. 191–204.

Leopold, E.B., and Denton, M.F., 1987, Comparative age of grassland and steppe east and west of the northern Rocky Mountains: Annals of the Missouri Botanical Garden, v. 74, p. 841–867.

Leopold, E.B., Reinink-Smith, L., and Mustoe, G.E., 2007, A deciduous forest pollen from the Wilkes Formation (Miocene) of southwest Washington: Geological Society of America Cordilleran Section 103rd Annual Meeting, Bellingham, Washington, May 4–6, 2007, abstract 20-9.

McWilliams, W.H., Tansey, J.B., Birch, T.W., and Hansen, M.H., 1998, *Taxodium-Nyssa* (Cypress-Tupelo) forests along the coast of the southern United States, *in* Laderman, A.D., ed., Coastally Restricted Forests: Oxford University Press, New York, p. 257–270.

Mozley, P.S., 1989, Relation between depositional environment and the elemental composition of early diagenetic siderite: Geology, v. 17, p. 704–706.

Mullineaux, D.R., Garde, L.M., and Crandall, D.R., 1959, Continental sediments of Miocene age in Puget Sound lowland, Washington: American Association of Petroleum Geologists Bulletin, v. 43, p. 688–696.

Mustoe, G.E., 2001, Enigmatic origin of ferruginous "coprolites:" Evidence from the Miocene Wilkes Formation, southwestern Washington: Geological Society of America Bulletin, v. 113, p. 673–681.

Mustoe, G.E., Leopold, E.B, Yancey, T.E., and Reinink-Smith, L., 2009, The Wilkes Formation: Using stratigraphy and paleobotany to study the effects of ancient volcanic activity on a Miocene forest: Eighth British Columbia Paleontological Association Symposium, University of British Columbia May 15–18, Abstract P-5.

Pierson, T.C., 2005, Hyperconcentrated flow: Transitional process between water flow and debris flow, *in* Jakob, M., and Hungr, O., eds., Debris Flow Hazards and Related Phenomena: Springer Praxis Books, Heidelberg, Germany, p. 159–202.

Reiners, P.W., Ehlers, T.A., Garver, J.I., Mitchell, S.G., Montgomery, D.R., Vance, J.A., and Nicolescu, S., 2002, Late Miocene exhumation and uplift of Washington Cascade Range: Geology, v. 30, p. 767–770.

Roberts, A.E., 1958, Geology and coal resources of the Toledo-Castle Rock district, Cowlitz and Lewis counties, Washington: U.S. Geological Survey Bulletin 1062, 71 p.

Scott, K.M., 1988, Origins, behavior, and sedimentology of lahars and lahar run-out flows in the Toutle-Cowlitz River system, Mount St. Helens, Washington: U.S. Geological Survey Professional Paper 1447A, p. 1–74.

Seilacher, A., Marshall, C., Skinner, C.W., and Tsuihiji, T., 2001, A fresh look at sideritic "coprolites": Paleobiology, v. 27, p. 7–13.

Smiley, C.J., 1963, The Ellensburg flora of Washington: University of California Publications in Geological Science, v. 35, p. 159–276.

Smith, G.A., 1988, Neogene synvolcanic and syntectonic sedimentation in central Washington: Geological Society of America Bulletin, v. 100, p. 1479–1492.

Smith, G.A., Campbell, N.P., Deacon, M.W., and Shafiqullah, M., 1988, Eruptive style and location of volcanic centers in the Miocene Cascade Range: Reconstruction from the sedimentary record: Geology, v. 16, p. 337–340.

Snaveley, P.D., Jr., Brown, R.D., Roberts, A.E., and Rau, W.W., 1958, Geology and coal resources of the Centralia-Chehalis district, Washington: U.S. Geological Survey Bulletin 1053, 159 p.

Spencer, P.K., 1993, The "coprolites" that aren't: The straight poop on specimens from the Miocene of southwestern Washington: Ichnos, v. 2, p. 231–236.

Tolan, T.L., Reidel, S.P., Beeson, M.H., Anderson, J.L., Fecht, K.R., and Swanson, D.A., 1989, Revisions to the estimates of the aerial extent and volume of the Columbia River Basalt Group, *in* Reidel, S.P., and Hooper, P.R., eds., Volcanism and Tectonism in the Columbia River Flood-basalt Province: Geological Society of America, Boulder, Colorado, Special Paper 239, p. 1–20.

Wells, R.E., Simpson, R.W., Bentley, R.D., Beeson, M.H., Mangan, M.T., and Wright, T.L., 1989, Correlation of Miocene flows of the Columbia River Basalt Group from the central Columbia River Plateau to the coast of Oregon and Washington, *in* Reidel, S.P., and Hooper, P.R., eds., Volcanism and Tectonism in the Columbia River Flood-basalt Province: Geological Society of America, Boulder, Colorado, Special Paper 239, p. 1–20.

Wolfe, J.A., 1987, An overview of the origins of the modern vegetation and flora of the northern Rocky Mountains: Annals of the Missouri Botanical Garden, v. 74, p. 785–803.

Wolfe, J.A., and Hopkins, D.M., 1967, Climatic changes recorded by Tertiary land floras in northwestern North America, *in* Hatai, K., ed., Tertiary Correlations and Climate Changes in the Pacific: Sasaki Publishers, Tokyo, p. 67–76.

Yamaguchi, D.K., and Hoblitt, R.P., 1995, Tree-ring dating of pre-1980 volcanic flowage deposits at Mount S. Helens, Washington: Geological Society of America Bulletin, v. 107, p. 1077–1093.

Yancey, T.E., and Mustoe, G.E., 2007, Depositional environments of the Wilkes Formation at Salmon Creek Washington: Source of siderite "coprolite" concretions: Geological Society of America Cordilleran Section103rd Annual Meeting, Bellingham, Washington, May 4–6, 2007, abstract 1-9.

ACCEPTED APRIL 30, 2013